Optimization of Strong and Weak Coordinates

MARCEL SWART, F. MATTHIAS BICKELHAUPT

Theoretische Chemie, Vrije Universiteit Amsterdam, De Boelelaan 1083, 1081 HV Amsterdam, The Netherlands

Received 19 July 2005; accepted 6 December 2005
Published online 4 April 2006 in Wiley InterScience (www.interscience.wiley.com).
DOI 10.1002/qua.21049

ABSTRACT: We present a new scheme for the geometry optimization of equilibrium and transition state structures that can be used for both strong and weak coordinates. We use a screening function that depends on atom-pair distances to differentiate strong coordinates from weak coordinates. This differentiation significantly accelerates the optimization of these coordinates, and thus of the overall geometry. An adapted version of the delocalized coordinates setup is used to generate automatically a set of internal coordinates that is shown to perform well for the geometry optimization of systems with weak and strong coordinates. For the Baker test set of 30 molecules, we need only 173 geometry cycles with PW91/TZ2P calculations, which compares well with the best previous attempts reported in literature. For the localization of transition state structures, we generate the initial Hessian matrix, using appropriate force constants from a database. In this way, one avoids the explicit computation of the Hessian matrix.
 Int J Quantum Chem 106: 2536–2544, 2006

Key words: geometry optimization; delocalized coordinates; intermolecular interactions; intramolecular interactions; weak interactions; density functional theory

Introduction

Knowledge of molecular structure is the basis from which we can proceed with attempting to understand chemistry and molecular biology. It is therefore a vital part of scientific studies into the details of chemical and physical phenomena. By now, molecular structures can be routinely obtained through experimental techniques, such as X-ray diffraction at crystals or nuclear magnetic resonance (NMR) spectroscopy, for molecules ranging in size from a few atoms to biomolecules of several thousands of atoms. There are limitations, however, to the applicability and accuracy of these experimental methods, for example, if crystallization is problematic. Moreover, reactive intermediates are often of key interest but too short-lived for experimental characterization. An example is compound I [1], supposedly one of the key intermedi-

Correspondence to: M. Swart; e-mail: m.swart@few.vu.nl
Contract grant sponsor: Scientific Research (NWO-CW).
This article contains supplementary material available via the Internet at http://www.interscience.wiley.com/jpages/0020-7608/suppmat/.

ates in the catalytic cycle of cytochrome P-450 enzymes [2]. The same problem but in amplified form exists for transition states of elementary chemical reaction steps. In general, reactive intermediates and transition states escape from direct experimental observation. A way out of this problem is provided by quantum chemistry which allows for computing the energy of any geometric configuration of a given set of atoms and, thus, also of all stationary points on the energy hypersurface [3]. An essential contribution to the successes of quantum chemistry (after the obviously important improvements in the accuracy of the quantum chemical methods themselves) comes from the ongoing development of still better, i.e., more efficient and numerical accurate techniques for the optimization of molecular geometries.

The most accurate class of standard quantum chemical models comprises coupled cluster methods which by now can be used (almost) routinely; coupled cluster theory is however limited to small- to medium-size molecules (on the order of 10–20 atoms). More widely used are density functional theory (DFT) [4–6] methods, which are more efficient and which can treat large systems, with an accuracy that approaches that of the coupled cluster methods. It was shown for the geometries of a set of small molecules that coupled cluster has an accuracy of ~0.1–0.4 pm [7, 8], while the best DFT functionals [9] follow closely with accuracies of 0.8–1.0 pm [9, 10]. In a recent study [11], we compared DFT and coupled cluster for the energy profiles of bimolecular nucleophilic substitution (S_N2) reactions; the coupled cluster data were taken from literature, and consisted of CCSD(T) energies with basis sets ranging from LanL2DZ to aug-cc-pV5Z. Our study showed that for the best DFT functionals, the average deviation from the coupled cluster reference data improves with basis set size, and approaches chemical accuracy (1 kcal/mol).

Quantum chemical methods are applied in many cases for the study of strong (intramolecular) interactions, i.e., "regular" chemical bonds, such as C—H or C—C. The treatment of weak (intermolecular) interactions, for example, hydrogen bonds, appears to be more difficult, both for the description of the interactions and for the optimization of the geometry parameters or coordinates involved. In the present study, we present a methodology for accurately and efficiently optimizing the molecular geometry of systems comprising weak interactions or strong interactions, or a combination of both.

Choice of Coordinate System

The performance of geometry optimization techniques depends critically on the choice of coordinates to be used in the optimization scheme. Although the use of $3N$ (N is the number of atoms) Cartesian coordinates is simple and straightforward, it is not the best choice for the optimization, as the individual components are too strongly coupled. For example, the Hessian, i.e., the matrix containing the second derivatives of the energy with respect to a complete set of coordinates, is dense in the case of Cartesian coordinates. Better performances are obtained by using Z-matrix coordinates [3]. They represent a predefined set of bond distances, angles and dihedrals that as a whole uniquely determines the atomic coordinates, and which has an almost diagonal Hessian matrix. However, the performance of the Z-matrix depends critically on its definition, and can, when chosen unfavorably, be even worse than that of Cartesian coordinates. Improved results may be obtained by using natural internal coordinates [12–14], which in essence is a combined set of bonds, angles, and dihedrals (the primitives), which are chosen based on the actual geometry of the molecule to be studied. However, the choice of which primitives to include, and with which weight factor, is still a matter of "hand work." It is therefore quite complicated, and can take several thousands of lines of computer code. An important step forward was made by the generation of delocalized coordinates, as formulated by Baker and coworkers [15–17].

In the delocalized coordinates setup [15–17], the weight factors follow naturally from the actual geometry. Starting from a set of primitives, containing all bonds, angles, and dihedrals of connected atoms, the usual B matrix [18, 19], relating the M primitives (Δq) with the corresponding $3N$ Cartesian displacements (Δx), is constructed [with $\mathbf{w}_p$, a diagonal matrix containing a weight factor for each primitive, see Eqs. (7)–(10) below]:

$$\mathbf{\Delta q} = \mathbf{w}_p\mathbf{B}\mathbf{\Delta x} = \mathbf{B}_p\mathbf{\Delta x}. \quad (1)$$

Then the $M \times M$ matrix $\mathbf{G} = \mathbf{B}_p\mathbf{B}_p^T$ is formed and diagonalized, which results in two sets of eigenvectors ($\mathbf{U}$ and $\mathbf{R}$); the first set ($\mathbf{U}$) of $3N-6$ (for linear molecules $3N-5$) nonredundant eigenvectors with eigenvalue $\lambda > 0$, and the second set ($\mathbf{R}$) of redundant eigenvectors with eigenvalue zero. The eigenvalue equation of $\mathbf{G}$ can thus be written as:

$$\mathbf{G(UR)} = \mathbf{(UR)}\begin{pmatrix}\mathbf{\Lambda} & \mathbf{0}\\ \mathbf{0} & \mathbf{0}\end{pmatrix}. \quad (2)$$

Only the first set of nonredundant eigenvectors (the set of active coordinates of the vectors contained in **U**) is needed for the geometry optimization, and contains the weights for each of the primitives. The *B* matrix is then transformed from primitive space to the active delocalized space ($\mathbf{B}_d = \mathbf{U}^T\mathbf{B}_p$), and the "inverse" *B* matrix is formed that transforms the Cartesian gradient to the delocalized gradient:

$$(\mathbf{B}_d^T)^{-1} = (\mathbf{B}_d\mathbf{B}_d^T)^{-1}\mathbf{B}_d$$
$$\mathbf{g} = (\mathbf{B}_d^T)^{-1}\mathbf{g}_{\text{cart}}. \quad (3)$$

Although the "inverse" *B* matrix could also be used to transform the Cartesian Hessian to delocalized space, it is more advantageous to start from the Hessian matrix in primitive space ($\mathbf{H}_p$). In this way, one can choose for each primitive coordinate individually a force constant [see Eq. (12) below] that is appropriate for that particular coordinate. This matrix $\mathbf{H}_p$ is then transformed to our active optimization space according to $\mathbf{H} = \mathbf{U}^T\mathbf{H}_p\mathbf{U}$.

The optimization procedure is then carried out within the active delocalized space, using the coordinates $\mathbf{s} = \mathbf{U}^T\mathbf{q}$ within the delocalized space, together with the gradient **g** and the Hessian **H**. After a step has been taken in the delocalized space, new Cartesian coordinates have to be formed involving a nonlinear back-transformation, which is solved in an iterative fashion [16]:

$$\mathbf{X}(k+1) = \mathbf{X}(k) + (\mathbf{B}_d^T)^{-1}(k)[\mathbf{s} - \mathbf{s}(k)]. \quad (4)$$

A more efficient way to solve this [17] is by first choosing an intermediate Z-matrix, as subset of the primitive coordinates **q**, which is sufficient to completely determine the Cartesian coordinates and that is used only in the back-transformation, and then iterate the primitive coordinates:

$$\mathbf{q}(k+1) = \mathbf{q}(k) + \mathbf{U}[\mathbf{s}^T - \mathbf{s}(k)^T]. \quad (5)$$

From the current estimate of **q**, new Cartesian coordinates **X** are obtained through the Z-matrix back-transformation, which lead to new values for the primitives **q** and subsequently to new values for the internal coordinates $\mathbf{s}(k) = \mathbf{U}^T\mathbf{q}$; these are then compared with the known **s**, and the difference used to obtain an improved estimate for **q**. In the current implementation, we construct the Z-matrix automatically in such a way as to include all coordinates with the largest weights.

Strong Versus Weak Coordinates

The delocalized coordinates setup works extremely well for strong coordinates, however, it was not yet designed for weak, e.g. intermolecular, coordinates. In another paper [20], Baker and Pulay proposed to use inverse-power distance coordinates for weak interactions such as present in a cluster of argon atoms. They tested both a/r and a/r^6 coordinates (with a scaling factor *a*), and found the a/r coordinate (with a scaling factor $a = 5$) to perform reasonably well for argon. In an attempt to generalize their results, we explored using $b(R_i+R_j)f(r)$, with a scaling factor *b*, a radius R_k that should be representative for atom *k* (either covalent or van der Waals radius), and different choices for the function $f(r)$; either r^{-1}, $\log(r)$, $r^{1/2}$, or $r^{-1/2}$. However, neither option performed satisfactorily.

Improved results were obtained by adding a weight to each primitive coordinate to separate them into strong and weak coordinates, as proposed by Lindh and coworkers [21]. These investigators used a model function to generate the weight, which they took from an earlier paper [22] that dealt with initial Hessian matrices based on parameterized force constants. As the early paper formulated the force constants only for the first three rows, and contains 15 parameters that were deduced from STO-3G Hartree–Fock calculations, we decided exploring a generalized form that depends also on the actual geometry of the molecule. We use for each atom pair in the primitive coordinates a screening function ρ_{ij}, that monitors the degree of covalence:

$$\rho_{ij} = \exp\{-[(r_{ij}/C_{ij}) - 1]\}, \quad (6)$$

in which r_{ij} is the distance between atoms *i* and *j*, and C_{ij} the sum of their covalent radii. The screening function is around one for atoms that are covalently bonded, and lower for weaker coordinates; all bonds with a screening function of ≥ 0.7 are considered strong bonds, the other bonds are weak. The weights for the different primitive coordinates is then obtained as

$$w = \rho_{ij} \qquad \text{bond } i\text{-}j \quad (7)$$

$$w = (\rho_{ij}\rho_{jk})^{1/2}[f + (1-f)\sin\theta_{ijk}] \qquad \text{angle } i\text{-}j\text{-}k,\ \theta_{ijk} \tag{8}$$

$$w = (\rho_{ij}\rho_{jk}\rho_{kl})^{1/3}[f + (1-f)\sin\theta_{ijk}][f + (1-f)\sin\theta_{jkl}] \qquad \text{dihedral } i\text{-}j\text{-}k\text{-}l \tag{9}$$

$$w = (\rho_{ij}\rho_{jk}\rho_{jl})^{1/3}[f + (1-f)\sin\theta_{ijk}][f + (1-f)\sin\theta_{ijl}] \qquad \text{improper } i\text{-}j\text{-}k\text{-}l \tag{10}$$

The parts involving the sine function have been included to disfavor (near-)linear angles, and include a damping factor f (which has a value of 0.12 in the current implementation). All coordinates with a weight above a certain threshold (currently 0.3) are included in the primitive space, all others do not contribute significantly and can be left out without problems.

Optimization Steps

Optimization techniques rely on a Taylor expansion of the energy E about the atomic coordinates X[3], which is usually cut off at second order:

$$E_{k+1} = E_k + \mathbf{g}^T\mathbf{X} + \mathbf{X}^T\mathbf{H}\mathbf{X} + \cdots. \tag{11}$$

Close to a minimum, the energy surface will be quadratic, and as a result, the best guess for the step to take is given by the Newton–Raphson step $\Delta\mathbf{X} = -\mathbf{H}^{-1}\mathbf{g}$. The success of the step depends critically on the accuracy of the curvature of the energy surface, i.e., the Hessian matrix, which should best be recalculated at every step in terms of number of geometry cycles. It is more cost-effective [19], however, to use an approximate Hessian $\mathbf{H}_a$, with the corresponding quasi-Newton step $\Delta\mathbf{X} = -\mathbf{H}_a^{-1}\mathbf{g}$. This will lead to an increase of the number of geometry cycles, but as the Hessian does not have to be calculated, it will also result in a decrease in the actual time used, saving in practice up to 84% of computer time [19].

Only close to the minimum is the energy surface actually quadratic, and can the Taylor expansion up to second order be trusted to be valid; this region is called the trust region, with a radius τ. If the quasi-Newton (QN) or Newton–Raphson (NR) step is smaller than τ, the QN/NR step is taken, else the restricted second order (RSO [23], also called level-shifted trust-region Newton method) [19] model is used. In the RSO model [23], a step is taken on the hypersphere of radius τ, using a Lagrange multiplier to ensure that the step length equals τ.

Although at every point the QN/NR step is the best option, the geometry optimization is enhanced by using GDIIS [24]; although the original paper proposed using the step as error vector, later studies showed it is more effective to use the gradient as error vector [25]. Furthermore, Farkas and Schlegel [26] have proposed a set of four rules that the GDIIS vectors have to fulfill. We have implemented the option to use either the step, the gradient or the "energy" vector (e.g., $B_{ij} = \mathbf{g}_i^T\mathbf{H}_k^{-1}\mathbf{g}_j$) [25] as error vector, and either with or without the Farkas–Schlegel rules; we observed the best performance by using the gradient as error vector, with a maximum of five GDIIS vectors, and imposing the Farkas–Schlegel rules.

Initial Hessian

The number of geometry cycles needed for convergence depends largely on the startup Hessian that is being used. Baker [16] proposed a simple scheme, using values of 0.5, 0.2, and 0.1 for bonds, angles, and dihedrals, respectively, which seems to work well for systems containing strong coordinates only. Lindh et al. [22] proposed reduced values of 0.45, 0.15, and 0.005, which are scaled with factors depending on the actual geometry. The ADF program uses force constant values by Fischer and Almlöf [27]. All these schemes have been implemented and tested, but we finally decided to adapt the scheme by Lindh et al. [22] and reuse the screening factors from Eq. (6), which leads to improved performance with the following adapted force constant values:

$$\begin{aligned} k_{\text{bond}} &= 0.35 \cdot \rho_{ij} \\ k_{\text{angle}} &= 0.15 \cdot \rho_{ij}\rho_{jk} \\ k_{\text{dihedral}} &= 0.005 \cdot \rho_{ij}\rho_{jk}\rho_{kl} \\ k_{\text{improper}} &= 0.005 \cdot \rho_{ij}\rho_{jk}\rho_{jl}\,. \end{aligned} \tag{12}$$

The use of the Hessian in primitive space also allows us to generate an appropriate starting Hessian for transition state searches, when starting from a reasonable guess structure and when the coordinates involved in the reaction coordinate (designated "RC coordinates") are known, which is usually the case. Along the RC coordinates, the energy achieves a maximum and the corresponding force

constants should thus be negative. Moreover, along the RC coordinates, in proximity to the transition state, the Hessian must have one (and only one) negative eigenvalue. This can be achieved by using a damped negative force constant value in the primitive Hessian for the RC coordinates; the force constants are damped with a factor 0.25 to result in a small negative Hessian eigenvalue. While in all other cases the primitive Hessian has all off-diagonal elements zero, we assign off-diagonal elements (between the RC coordinates only!) in this case to couple the RC coordinates, which is crucial for describing the reaction coordinate. The values for the off-diagonal elements are chosen in order to result in only one negative eigenvalue (the rest positive), which can be achieved by using $H_{p,ij} = H_{p,ji} = -(2H_{p,ii}H_{p,jj})^{1/2}$ (the minus sign serves to obtain the plus combination for the eigenvector of the negative eigenvalue). During the optimization, the Hessian is updated using either the BFGS (for minima) or Bofill (for transition state) update schemes (see Ref. [19] for details).

Density Functional Theory

The generation of the delocalized coordinates, screening functions, etc., and the actual geometry optimization scheme was performed within the QUantum regions Interconnected by Local Descriptions (QUILD) [28] program, which has been developed for QM/QM calculations, and which functions as a wrapper around the ADF program [29]. The QUILD program constructs all input files for ADF, runs ADF, and collects all data; ADF is used only for the generation of the energy and gradients.

All DFT calculations were performed with the Amsterdam Density Functional (ADF, version 2004.01) program developed by Baerends and coworkers [29, 30]. The MOs were expanded in a large uncontracted set of Slater-type orbitals (STOs) (TZ2P) [31], which is of triple-ζ quality, augmented by two sets of polarization functions (e.g., 3*d* and 4*f* on C, N, O; 2*p* and 3*d* on H); the core electrons (e.g., 1*s* for the second period, 1*s*2*s*2*p* for the third period) were treated by the frozen-core (FC) approximation [30]. An auxiliary set of *s*, *p*, *d*, *f*, and *g* STOs was used to fit the molecular density and to represent the Coulomb and exchange potentials accurately in each self-consistent field (SCF) cycle.

Energies and gradients were calculated using the local density approximation (LDA; Slater exchange and VWN [32] correlation) with nonlocal (PW91 [33, 34]) corrections added self-consistently. This xc-functional is one of the best DFT functionals for the accuracy of geometries [9], with an estimated unsigned error of 0.8 pm in combination with the TZ2P basis set. Furthermore, it is able to treat weak interactions correctly [35]. For the determination of transition state structures, the OPBE [10] functional has been used, as it has been shown recently [11] to be the best performing functional for the energy surfaces of nucleophilic substitution (S_N2) reactions.

Results for Strong Coordinates: Baker Test Set

Baker [36] proposed a test set of 30 molecules (see Fig. S1 in the Supporting Information) that can be used for comparing different optimization strategies, with a convergence criterion for the gradient of $3.0 \cdot 10^{-4}$. The starting geometries have been obtained from the supporting information in the paper by Bakken and Helgaker; however, the latter study contains two small typographical errors (for ACANIL01 and neopentane); therefore, the corrected coordinates are given in the supporting information of this contribution. Table I collects the results for a number of different geometry optimization schemes including our method (in the last column). The total number of geometry cycles needed with quasi-Newton methods ranges from 240 (Baker [36]), 196 (Eckert et al. [25]), and 215 (Lindh et al. [22]) to 185 (Bakken and Helgaker [19]). Note that the latter number can be reduced to 111, when the exact Hessian is used at every step [19].

Our value of 173 geometry cycles (obtained at PW91/TZ2P using a convergence criterion of $3.0 \cdot 10^{-4}$ a.u.) is slightly better than that of Bakken and Helgaker. We would like to point out, however, that a direct comparison of our values with those from the literature bears some problems because totally different methods have been used in either case. It is unclear a priori whether the use of the PW91 method is an advantage or a disadvantage compared to the simple RHF/STO-3G. However, it is comforting that the total number of geometry cycles is comparable to the best effort from the literature using the RHF method.

TABLE I

Number of geometry cycles for optimizing molecules of the Baker test set, compared for various geometry optimization schemes.

Molecule	Baker [36][a]	Lindh [22][a]	Eckert [25][a]	Bakken [19][a]	This work[b]
Water	6	4	4	4	4
Ammonia	6	5	6	5	4
Ethane	5	4	4	3	4
Acetylene	6	5	6	4	4
Allene	5	5	4	4	4
Hydroxysulfane	8	8	7	7	6
Benzene	4	3	3	3	3
Methylamine	6	5	5	4	4
Ethanol	6	5	5	4	5
Acetone	6	5	5	4	5
Disilyl-ether	8	11	9	8	8
1,3,5-Trisilacyclohexane	8	8	6	9	6
Benzaldehyde	6	5	5	4	5
1,3-Difluorobenzene	5	5	5	4	4
1,3,5-Trifluorobenzene	5	4	4	4	4
Neopentane	5	5	4	4	4
Furan	8	7	6	5	5
Naphthalene	5	6	6	5	5
1,5-Difluoronaphthalene	6	6	6	5	5
2-Hydroxybicyclopentane	15	10	9	9	10
ACHTAR10	12	8	9	8	8
ACANIL01	8	8	8	7	5
Benzidine	9	10	7	9	6
Pterin	10	9	9	8	8
Difuropyrazine	9	7	7	6	8
Mesityl-oxide	7	6	6	5	5
Histidine	19	20	14	16	14
Dimethylpentane	12	10	10	9	5
Caffeine	12	7	7	6	7
Menthone	13	14	10	12	8
Sum	240	215	196	185	173
Rounded average	8	7	7	6	6

[a] RHF/STO-3G.
[b] PW91/TZ2P.

Results for Weak Coordinates

Table II reports our results for a set of 12 systems (see Fig. 1), which involve both weak and strong coordinates. Apart from the water–hydronium system, all systems converge within 30 cycles to a gradient of $1.0 \cdot 10^{-5}$ a.u., which is a good result, given the relatively flat energy surfaces. The relatively poor performance for the water–hydronium system might be the result of its somewhat distorted starting structure, but also then should the optimization scheme be able to find the minimum

TABLE II

Number of geometry cycles for optimizing the geometry of systems involving weak coordinates with our geometry optimization scheme.*

Molecule	Iterations	Molecule	Iterations
Ar···Ar	7	$H_2O\cdots H_3O^+$	40
$CH_4\cdots CH_4$	8	$H_2O\cdots NH_3$	13
$CH_4\cdots NH_3$	9	$H_2O\cdots NH_4^+$	22
$F^-\cdots HF$	6	$HF\cdots H_2O$	11
$H_2O\cdots H_2O$	11	$NH_3\cdots NH_3$	20
Cyt···Cyt (CC3)	16[a]	$CHBr_3\cdots H_2O_2$	29

* PW91/TZ2P results.
[a] BP86/DZP result.

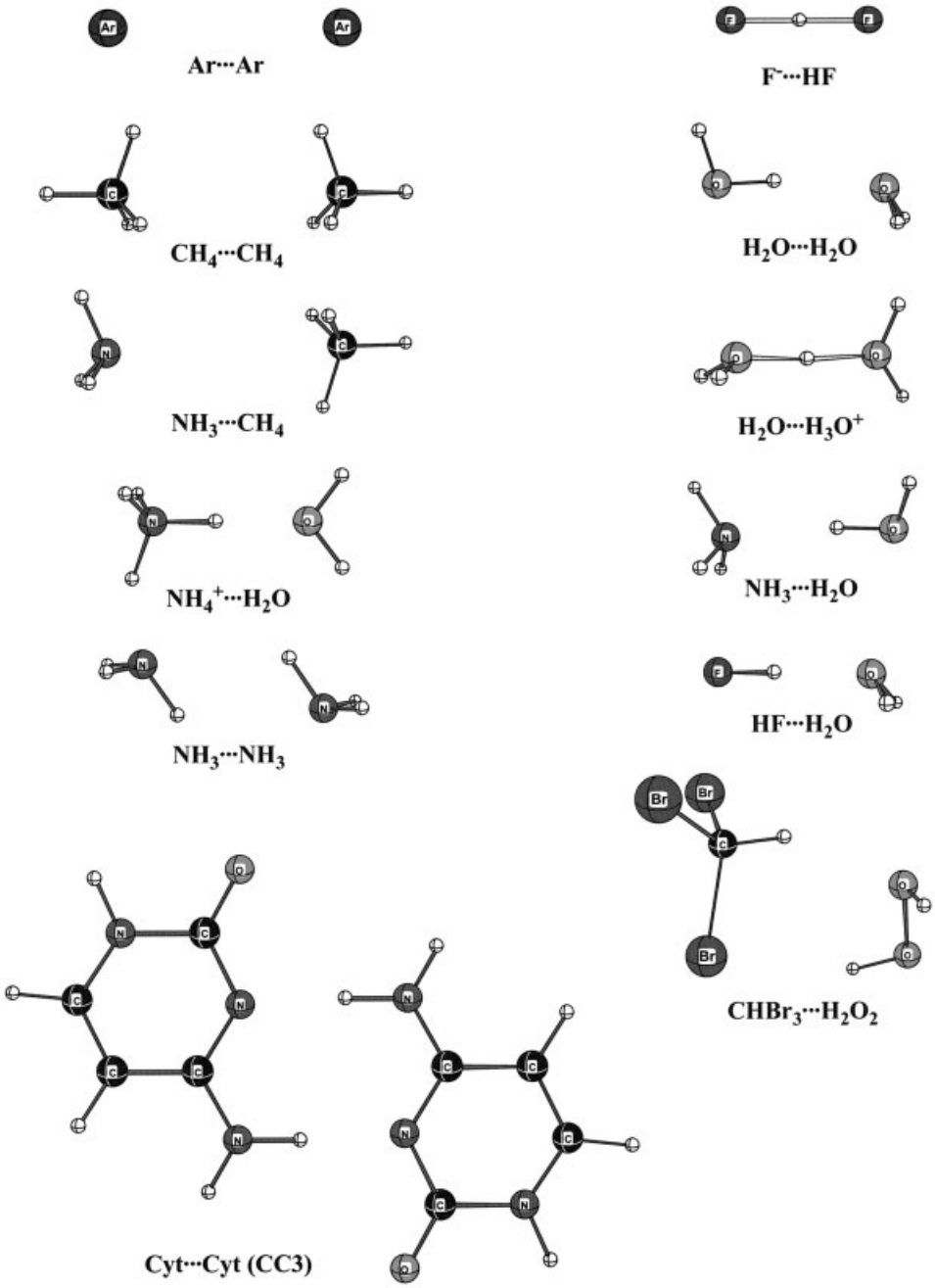

FIGURE 1. Optimized structures (PW91/TZ2P) of weak coordinate systems.

structure, as it clearly does, although with a slight increase of the number of cycles needed. The overall average number of geometry optimization cycles required for our test set of 12 molecules is 16. This is nearly 3 times higher than the average number of geometry optimization cycles that we need in the case of the Baker test set. This can be ascribed to the stricter convergence criterion for the gradient ($1.0 \cdot 10^{-5}$ versus $3.0 \cdot 10^{-4}$) and also, at least in part, to the fact that optimization of the weak coordinates which are associated with shallow potential energy surfaces is computationally more involved. Note however that the difference should not be overinterpreted, as it may, and probably is, affected also by ill-defined differences in chosen starting geometries.

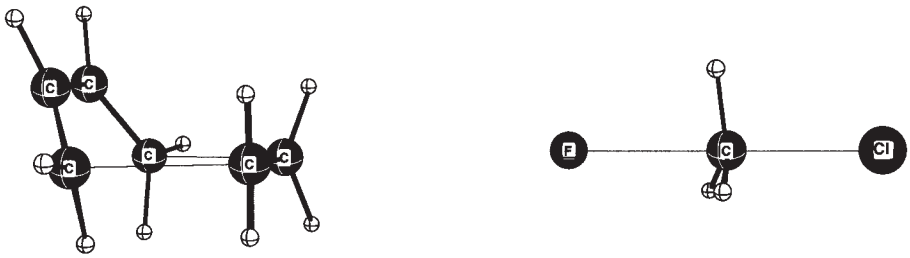

FIGURE 2. Optimized transition state structures (OPBE/TZ2P) of the Diels–Alder and S_N2-reaction.

Interestingly, both our proposed weight function for primitive coordinates and the corresponding force constants seem to work well, for weak interactions of different strength: both for the donor–acceptor interaction of fluoride-hydrogen fluoride, dipole-induced dipole of methane-ammonia, and induced dipole-induced dipole of the methane and argon dimers do we find the minimum structure within 10 geometry cycles. For the argon dimer, we find an equilibrium distance of 3.9 Å and stabilization energy of 112 cm^{-1}, which compares well with CCSD(T) data of 3.8–3.9 Å and 70–100 cm^{-1} (obtained with basis sets ranging from aug-cc-pVTZ to extrapolation to basis set limit) [37].

We tested our setup for computing transition state structures using two prototypical reactions from organic chemistry (see Fig. 2), the parent Diels–Alder reaction of ethylene and butadiene, and the asymmetric nucleophilic substitution (S_N2) reaction of fluoride and methylchloride. The starting structures were taken from a PM3 (Diels–Alder) and CCSD(T)/TZ2Pf+dif (S_N2) [38] optimization. Our choice for the starting Hessian resulted, as anticipated, in it having one (and only one) negative eigenvalue of -0.017 and -0.160 a.u., respectively, for the Diels–Alder and the S_N2 reaction. With OPBE/TZ2P the transition state structure is optimized to a gradient of $1.0 \cdot 10^{-5}$ a.u. in, respectively, 11 (Diels–Alder) and 9 (S_N2) cycles. The partially formed C—C bond in the Diels–Alder reaction is then 2.337 Å, while in the S_N2 reaction the partially formed C—F and broken C—Cl bonds are 2.085 and 2.084 Å, respectively.

Conclusions

We have presented a new geometry optimization scheme for determining equilibrium and transition state structures, which is able to deal with both strong and weak coordinates on a consistent level. The current implementation constructs automatically a set of internal coordinates, using the delocalized coordinates setup by Baker and coworkers. Standard optimization techniques, such as a quasi-Newton step combined with GDIIS, are used to generate the steps. The initial Hessian is constructed by a generalization of Lindh's force constant model, which is exploited further for generating an appropriate initial Hessian in the case of transition state structures. The optimization scheme has been tested on systems with strong coordinates (the Baker test set), weak coordinates (involving, i.e., hydrogen bonds), and two transition state structures (Diels–Alder and S_N2 reactions). In all cases do we observe good performance of our scheme, with an average of six geometry cycles for the molecules in the Baker test set, 16 cycles for the weak-coordinate systems, and 10 for the transition state searches.

Supporting Information

Cartesian coordinates of the starting geometries and the final, converged geometries of all species involved.

References

1. Limberg, C. Angew Chem Int Ed 2003, 42, 5932.
2. Ortiz de Montellano, P. R. Cytochrome P-450 Structure, Mechanism and Biochemistry; Plenum: New York, 1995.
3. Jensen, F. Introduction to Computational Chemistry; Wiley & Sons: New York, 1998.
4. Parr, R. G.; Yang, W. Density Functional Theory of Atoms and Molecules; Oxford University Press: New York, 1989.

5. Koch, W.; Holthausen, M. C. A Chemist's Guide to Density Functional Theory; Wiley-VCH: Weinheim, 2000.
6. Dreizler, R.; Gross, E. Density Functional Theory; Plenum: New York, 1995.
7. Helgaker, T.; Gauss, J.; Jørgensen, P.; Olsen, J. J Chem Phys 1997, 106, 6430.
8. Bak, K. L.; Gauss, J.; Jørgensen, P.; Olsen, J.; Helgaker, T.; Stanton, J. F. J Chem Phys 2001, 114, 6548.
9. Swart, M.; Snijders, J. G. Theor Chem Acc 2003, 110, 34; Erratum: ibid 111, 156.
10. Swart, M.; Ehlers, A. W.; Lammertsma, K. Mol Phys 2004, 102, 2467.
11. Swart, M.; Solà, M.; Bickelhaupt, F. M. (in preparation) 2005.
12. Billeter, S. R.; Turner, A. J.; Thiel, W. Phys Chem Chem Phys 2000, 2, 2177.
13. Pulay, P.; Fogarasi, G. J Chem Phys 1992, 96, 2856.
14. von Arnim, M.; Ahlrichs, R. J Chem Phys 1999, 111, 9183.
15. Baker, J. J Comput Chem 1997, 18, 1079.
16. Baker, J.; Kessi, A.; Delley, B. J Chem Phys 1996, 105, 192.
17. Baker, J.; Kinghorn, D.; Pulay, P. J Chem Phys 1999, 110, 4986.
18. Wilson, E. B., Jr.; Decius, J. C.; Cross, P. C. Molecular Vibrations—The Theory of Infrared and Raman Vibrational Spectra; McGraw-Hill: New York, 1955.
19. Bakken, V.; Helgaker, T. J Chem Phys 2002, 117, 9160.
20. Baker, J.; Pulay, P. J Chem Phys 1996, 105, 11100.
21. Lindh, R.; Bernhardsson, A.; Schutz, M. Chem Phys Lett 1999, 303, 567.
22. Lindh, R.; Bernhardsson, A.; Karlstrom, G.; Malmqvist, P. A. Chem Phys Lett 1995, 241, 423.
23. Yeager, D. L.; Jensen, H. J. A.; Jørgensen, P.; Helgaker, T. U. In Geometrical Derivatives of Energy Surfaces and Molecular Properties; Jørgensen, P.; Simons, J., Eds.; Reidel: Dordrecht, The Netherlands, 1986; p 229.
24. Csaszar, P.; Pulay, P. J Mol Struct 1984, 114, 31.
25. Eckert, F.; Pulay, P.; Werner, H. J. J Comput Chem 1997, 18, 1473.
26. Farkas, O.; Schlegel, H. B. Phys Chem Chem Phys 2002, 4, 11.
27. Fischer, T. H.; Almlof, J. J. Phys. Chem. 1992, 96, 9768.
28. Swart, M.; Bickelhaupt, F. M. Amsterdam, 2005.
29. Baerends, E. J.; Autschbach, J.; Bérces, A.; Bo, C.; Boerrigter, P. M.; Cavallo, L.; Chong, D. P.; Deng, L.; Dickson, R. M.; Ellis, D. E.; Fan, L.; Fischer, T. H.; Fonseca Guerra, C.; Van Gisbergen, S. J. A.; Groeneveld, J. A.; Gritsenko, O. V.; Grüning, M.; Harris, F. E.; van den Hoek, P.; Jacobsen, H.; van Kessel, G.; Kootstra, F.; van Lenthe, E.; McCormack, D. A.; Osinga, V. P.; Patchkovskii, S.; Philipsen, P. H. T.; Post, D.; Pye, C. C.; Ravenek, W.; Ros, P.; Schipper, P. R. T.; Schreckenbach, G.; Snijders, J. G.; Solà, M.; Swart, M.; Swerhone, D.; te Velde, G.; Vernooijs, P.; Versluis, L.; Visser, O.; van Wezenbeek, E.; Wiesenekker, G.; Wolff, S. K.; Woo, T. K.; Ziegler, T. SCM: Amsterdam, 2004.
30. te Velde, G.; Bickelhaupt, F. M.; Baerends, E. J.; Fonseca Guerra, C.; van Gisbergen, S. J. A.; Snijders, J. G.; Ziegler, T. J Comput Chem 2001, 22, 931.
31. van Lenthe, E.; Baerends, E. J. J Comput Chem 2003, 24, 1142.
32. Vosko, S. H.; Wilk, L.; Nusair, M. Can J Phys 1980, 58, 1200.
33. Perdew, J. P. In Electronic Structure of Solids 1991; Ziesche, P.; Eschrig, H., Eds.; Akademie: Berlin, 1991; p 11.
34. Perdew, J. P.; Chevary, J. A.; Vosko, S. H.; Jackson, K. A.; Pederson, M. R.; Singh, D. J.; Fiolhais, C. Phys Rev B 1992, 46, 6671.
35. Xu, X.; Goddard, W. A., III. Proc Natl Acad Sci USA 2004, 101, 2673.
36. Baker, J. J Comput Chem 1993, 14, 1085.
37. Slavicek, P.; Kalus, R.; Paska, P.; Odvarkova, I.; Hobza, P.; Malijevsky, A. J Chem Phys 2003, 119, 2102.
38. Gonzales, J. M.; Cox, R. S., III; Brown, S. T.; Allen, W. D.; Schaefer, H. F., III. J Phys Chem A 2001, 105, 11327.